

Mathematical description of concentric demyelination in the human brain: self-organization models, from Liesegang rings to chemotaxis

V. Calvez^{a *}, R. H. Khonsari^{b †}

^aDépartement de Mathématiques et Applications,
École normale supérieure, 45 rue d'Ulm, 75005 Paris, France
vincent.calvez@ens.fr

^bLaboratoire de Neuropathologie Raymond Escourolle,
Hôpital de la Pitié-Salpêtrière, 91–105 boulevard de l'Hôpital, 75013 Paris, France
hossein.khonsari@ens.fr

Baló's concentric sclerosis (BCS) is an atypical variant of multiple sclerosis (MS) characterized by remarkable concentric demyelination patterns in the white matter of the brain and the spinal chord. In Khonsari & Calvez (2006), we introduced a very simple model based on cellular self-organization, which reproduced quite accurately the quantitative and qualitative aspects of this disease. The present paper provides more details on the mathematical framework underlying our precedent work. We first review the basics of the chemotaxis aggregation principle and the modeling of the Liesegang rings (LR) phenomenon. We then present our local macrophages recruitment model, which derives from the reconsidering of the classical analogy between LR and BCS. This new model provides several non-obvious insights, such as the link between the level of aggressivity of the disease and the emergence of patterns.

Key words.

pattern formation, multiple sclerosis, concentric sclerosis, Liesegang rings, chemotaxis, volume-filling.

1. Introduction

Spatial cellular self-organization is a challenging area at the interface of mathematics and biology [50]. Biological phenomena involving self-organization are as different as bacterial colony growth [6,9,36], embryology [47], wound healing [19] and cancer growth [56,10]. The importance of chemical species in morphogenesis was first suggested by Alan Turing [60], who introduced the so-called diffusion-driven instability. Our personal approach is based on chemotaxis, which provides basic instabilities for collective aggregation [55]. It is probably one of the main phenomena explaining cellular spatial

*Corresponding author

†*Present address:* Service de chirurgie maxillo-faciale, Centre Hospitalier Universitaire de Nantes, 1 place Alexis Ricordeau, 44000 Nantes, France

organization. When dealing with a large number of cells, the models mainly involve parabolic PDEs [16], as it is for the Patlak, Keller & Segel model [54,37].

The biological phenomenon we study in this paper is the concentric demyelination occurring in a particular form of multiple sclerosis (MS), namely the Baló's concentric sclerosis (BCS). The pathogeny of BCS has been a neuropathologic enigma for many years. We suggested in a previous paper [39] that the robust patterns appearing in this disease may result from a chemotactic mechanism, involving three species.

$$\begin{aligned}
 \frac{\partial m}{\partial t} &= \underbrace{D\Delta m + \lambda m(\bar{m} - m)}_{\substack{\text{front of macrophages} \\ \text{activation}}} - \underbrace{\nabla \cdot (\chi m(\bar{m} - m)\nabla c)}_{\substack{\text{local recruitment} \\ \text{of macrophages}}} \\
 \frac{\partial d}{\partial t} &= \underbrace{F(m)m(\bar{d} - d)}_{\text{destruction of myelin}} \\
 \underbrace{-\varepsilon\Delta c + \alpha c}_{\substack{\text{production and fast diffusion} \\ \text{of the attracting signal}}} &= \mu d \quad ,
 \end{aligned} \tag{1.1}$$

The combined effects of the activating front propagation and aggregation lead to the formation of robust concentric bands of destroyed myelin (see section 5.2). Furthermore, as a consequence of the mathematical properties of our chemotaxis-based model, the striking patterns observed in BCS may be the result of the peculiar aggressivity of this pathology [39].

Interesting analogies between BCS and LR have been raised early in the literature [29]. In the following we present models inspired from these analogies, but adapted to the current discoveries on the cellular mechanisms of demyelination. The paper is organized as follows. We first introduce the basics of aggregation modeling and survey the state of the art in the Patlak, Keller & Segel model [54,37] (section 2). We then briefly describe the neuropathology of BCS (section 3, we refer to [39] for a more in-depth presentation). Section 4 introduces the Ostwald supersaturation scenario for the formation of Liesegang rings and the preconditioning model proposed by Stadelman et al. [58] for BCS. Finally, section 5 presents more refined models for concentric patterning by self-organization, namely the post-nucleation scenario for Liesegang rings and our local macrophage recruitment model.

2. Cellular self-organization and chemotaxis

Chemotaxis is the motion of cells in response to a chemical signal. It occurs for instance in tumoral angiogenesis [2,27,46] and in avian gastrulation during the formation of the primitive streak [65]. In the brain, chemotaxis is known to play a role in the neural migration that leads to cortical development [59]. Furthermore, cellular motion in immunologic response is directed by chemokines like $\text{TGF}\beta$ or $\text{INF}\gamma$. Chemotaxis may also be involved in the genesis of pigmentation patterns [52] (see also [28]).

When cells themselves are involved in the production of cell-attracting chemical signals, self-organization may occur. The simplest non-linear chemotaxis-based model is the Patlak, Keller & Segel (PKS) model for collective cellular aggregation. Many exciting research topics have emerged from this theory. This model involves only two variables: the cell density and the chemoattractant concentration. The core of PKS is the following nonlinear coupling: the amount of chemoattractant produced by the cells increases with the number of cells. Other models involving more realistic and complex kinetics have been proposed. For instance, in order to describe the aggregation phase in the amoebae *Dictyostelium discoideum*'s life cycle, the chemotaxis master equation has been coupled with a system of two reaction-diffusion equations involving traveling pulses in an excitable medium [33]. Related results have been obtained in [13] where a one-parameter family of smallness conditions is derived for existence of global solutions.

In the following subsection, we review classical PKS from a mathematical viewpoint. We aim to describe the chemotaxis aggregation principle involving, among other parameters, the total mass of cells. Next, we present recent theoretical developments taking into account density-dependent saturation effects on cellular movements (non-linear diffusion and/or saturation of the chemotactic response).

2.1. The classical PKS model – A brief overview

The PKS model has been introduced to describe the aggregation phase of a cellular population viewed as a continuum (bacterial colonies, aggregation phase in the life cycle of *Dictyostelium*). Depending on the modeling goals, several PKS variants have been proposed, involving for instance blow-up or traveling waves. Here, we only consider two species, namely the cell density $n(t, x)$ and the chemoattractant concentration $c(t, x)$, in dimension two. From Jäger and Luckhaus [35] we write, in the fast chemical diffusion case,

$$\begin{cases} \frac{\partial n}{\partial t} = D\Delta n - \nabla \cdot (\chi n \nabla c) & \text{in } \mathbb{R}^+ \times \Omega, \\ -\Delta c = \mu(n - \langle n \rangle), \end{cases} \quad (2.1)$$

$\Omega \subset \mathbb{R}^2$ being the domain under consideration, which can be a bounded domain or the full space \mathbb{R}^2 . In the former case, boundary conditions are zero flux,

$$\begin{cases} D \frac{\partial n}{\partial \eta} - \chi n \frac{\partial c}{\partial \eta} = 0 & \text{on } \partial\Omega, \\ \frac{\partial c}{\partial \eta} = 0, \end{cases}$$

η being the outwards unit normal vector to the domain boundary $\partial\Omega$. The compatibility correction $\langle n \rangle$ is the mean value of the cell density over the domain; it corresponds to Neumann boundary conditions for c in a bounded domain Ω and has zero value if Ω is the full space. In the full space, the Poisson equation $-\Delta c = \mu n$ has to be understood with c being

$$c = -\frac{\mu}{2\pi} \int_{\mathbb{R}^2} \log|x-y| n(t, y) dy. \quad (2.2)$$

We can adimensionalize the system (2.1) and we end up with only one reduced parameter,

$$\tilde{\chi} = \frac{\mu\chi M}{D}, \quad (2.3)$$

where M is the total mass of cells, conserved along time.

The qualitative behaviour of this model results from the balance between two opposite tendencies. The following alternative arises: either cells spread (when interactions are negligible), or they aggregate, that is the cell density blows up (cell-to-cell attraction dominates). The principle of mass constrain can be stated as follows: the reduced parameter $\tilde{\chi}$ drives the structure of the cellular population. If all the parameters of the dimensionalized model (2.1) are fixed, the amount of cells determines whether self-organization takes place or not.

Theorem 1 (Full space, [22]). *If Ω is the whole space \mathbb{R}^2 and the initial data satisfies $n_0(|\log n_0| + (1 + |x|^2)) \in L^1$, then solutions are global in time if $\mu\chi M/D < 8\pi$, or blow up in finite time if $\mu\chi M/D > 8\pi$.*

This theorem and its variants are due to several contributions, among which Jäger and Luckhaus [35], Biler and Nadzieja [7], Nagai [48], Gajewski and Zacharias [26], Dolbeault and Perthame [22].

Remark 2. *The alternative in the full space is simple because there is a single threshold. On a bounded domain, the boundary conditions imposed to the chemical species are crucial. For instance, Neumann boundary conditions lead to global existence under the condition $\mu\chi M/D < 4\pi$ because of boundary effects [7,26,34,12].*

The method for proving global existence in theorem 1 is based on the free energy associated with the system (2.3). In the adimensional form, the following quantity is time decreasing,

$$\mathcal{E}(t) = \int \tilde{n} \log \tilde{n} - \frac{\tilde{\chi}}{2} \int \tilde{n} \tilde{c}. \quad (2.4)$$

The proof involves the logarithmic Hardy-Littlewood-Sobolev inequality [15], which compares the opposite contributions of diffusion and chemical potential to cellular motion.

Remark 3 (PKS model in dimension $d \neq 2$). *At least two ways of generalizing the PKS model in dimensions other than two are possible, depending on the spatial law for chemical diffusion.*

- *First, one may keep the equation $-\Delta c = n$. The qualitative behaviour thus depends on the dimension: for $d = 1$, blow-up never occurs [48], but may happen in higher dimensions. In this case, the $L^{d/2}$ -norm is critical instead of the mass [18].*
- *Following (2.2), one may use the logarithmic interaction kernel and state $c = -\frac{1}{d\pi} \log |x| * n$. In this case, the qualitative picture is the same for every dimension d and the threshold is $2d^2\pi$ [14].*

2.2. Volume effects – Recent issues

Several approaches lead to volume effects in the chemotaxis equation. It is mathematically relevant to include nonlinear density-dependent coefficients in order to avoid non-realistic blow-up. From a modeling point of view, the pressure function may be overvaluated for high cell-density levels [27,40]. Another possibility is to come back to the biased random walk framework [1] and introduce a nonincreasing function q . This function takes into account that cellular motion is slowed down when cells are packed [53]. All these saturating effects are included in the following master equation,

$$\frac{\partial n}{\partial t} + \nabla \cdot \left(-n \nabla h(n) + \chi(n)n \nabla c \right) = 0, \quad (2.5)$$

$h(u)$ being the pressure function and $\chi(u)$ the density-dependent chemosensitivity. In addition we introduce the nonlinear reduced pressure function, defined by

$$H'(u) = \frac{h'(u)}{\chi(u)}, \quad H(1) = 0. \quad (2.6)$$

Theorem 4 (Volume effects, [11]). *Let $\Omega \subset \mathbb{R}^2$ be a bounded domain. We assume that H is growing to infinity faster than $\frac{\mu M}{4\pi} \log u$ for large u , that is there exists $\delta > 0$ and $\mathcal{U} \in \mathbb{R}_+$ such that*

$$\forall u \geq \mathcal{U}, \quad H(u) \geq \left(\frac{\mu M}{4\pi} + \delta \right) \log u. \quad (2.7)$$

Then, there are global solutions under suitable initial conditions.

Remark 5. *The criterion for blow-up prevention is the non-linear analogue of theorem 1. The non-linear reduced pressure (2.6) is involved in the balance between spread (high pressure) and cell-to-cell attraction (low pressure), instead of the reduced coefficient $\mu \chi M / D$. In fact theorem 4 reduces to theorem 1 because $h(u) = D \log u$ in the "linear case".*

The proof of theorem 4 also relies on refined estimations of the free energy,

$$\mathcal{E}(t) = \int \Phi(n) dx - \frac{\mu}{2} \int nc dx, \quad \text{with } \Phi \text{ defined as } \Phi'(u) = H(u), \Phi(0) = 0.$$

Examples and numerics

In the biased random walk approach, the density dependent transition rate q represents the saturation effects [53]. The relation between q and the nonlinear pressure and chemosensitivity functions in (2.5) is given by

$$\begin{cases} uh'(u) = D(q(u) - uq'(u)), \\ \chi(u) = \chi_0 q(u), \end{cases} \quad H'(u) = \frac{D}{\chi_0} \frac{q(u) - uq'(u)}{q(u)u}. \quad (2.8)$$

The overcrowding effect is illustrated by the following two generic examples (see also figure 1).

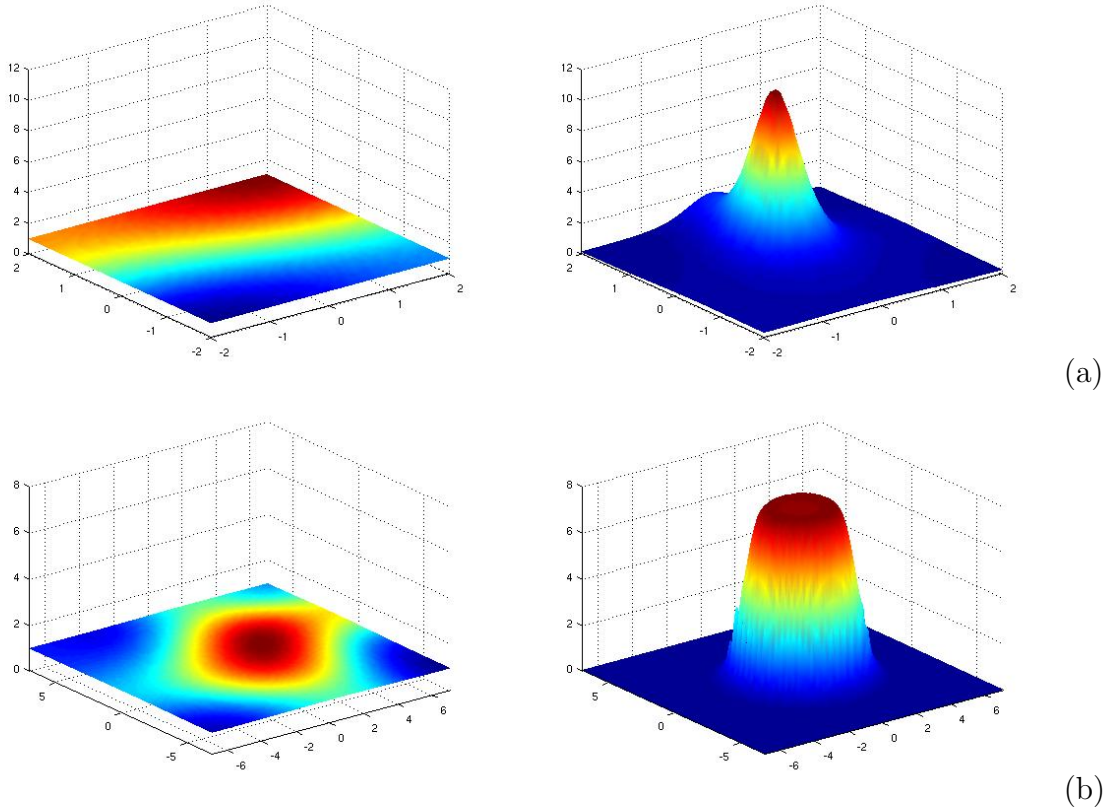


Figure 1. Illustration of the chemotaxis principle with volume effects: each figure corresponds to the final equilibrium state of the cell density (except in *top-right*, where blow-up occurs). Simulations are performed on a square regular grid using the discretization (2.11). (a) The transition rate is $q(u) = \frac{1}{1+u}$. The initial condition is a perturbation of a homogeneous cell population with density 1 and total mass $M = 16$. Other parameters are $D = 1$, $\mu = 1$ and (*left*) $\chi_0 = 2$, (*right*) $\chi_0 = 10$. For convenience, the right figure is an intermediate state: all the mass is finally concentrated at one point (blow-up). The situation is qualitatively close to the classical model, where blow-up occurs if $\mu\chi_0 M/D$ is sufficiently large. (b) We set $q(u) = e^{-u}$. The initial condition is a perturbation of a homogeneous cell population with density 1 and total mass $M = 200$. Other parameters are $D = 1$, $\mu = 1$ and (*left*) $\chi_0 = 2.6$, (*right*) $\chi_0 = 3$. Although the solutions do not blow-up, there is a transition in equilibria between the spread of cells and aggregation, where cell density is highly localized.

(a) If q has a polynomial decay, $q(u) = \frac{1}{1+u^\gamma}$, $\gamma > 0$, then we get

$$H'(u) = \frac{D}{\chi_0} \frac{1 + (\gamma + 1)u^\gamma}{u(1 + u^\gamma)} \sim_\infty \frac{D}{\chi_0} \frac{\gamma + 1}{u}. \quad (2.9)$$

In this case, the corresponding diffusion law is asymptotically linear, and blow-up is avoided if $D(1 + \gamma)/\chi_0 > \mu M/4\pi$.

(b) If q is exponentially decreasing as $q(u) = e^{-\beta u}$, $\beta > 0$, then we obtain

$$H'(u) = \frac{D}{\chi_0} \frac{1 + \beta u}{u} \sim_\infty \frac{D}{\chi_0} \beta. \quad (2.10)$$

Here, the reduced diffusion is asymptotically quadratic for large cell density and blow-up never occurs because the condition (2.7) is always verified.

Filbet [23] provided theoretical results on PKS numerics based on discrete functional inequalities. Here we adopt the Scharfetter & Gummel [57] factorization method for our numerical scheme. This method is common in the theory of semi-conductor devices, and gives a key role to the reduced pressure function. We rewrite the flux term of (2.5) as follows,

$$\frac{\partial n}{\partial t} = \nabla \cdot \left(Dq(n)^2 e^{\frac{\chi_0}{D}c} \nabla \left(\frac{n}{q(n)} e^{-\frac{\chi_0}{D}c} \right) \right). \quad (2.11)$$

Remark 6. Note that (2.11) is a particular case of the following computation

$$\begin{aligned} \frac{\partial n}{\partial t} &= \nabla \cdot \left(n\chi(n) \nabla (H(n) - c) \right) \\ &= \nabla \cdot \left(Dn \frac{\chi(n)}{\chi_0} e^{\frac{\chi_0}{D}c - \frac{\chi_0}{D}H(n)} \nabla \left(e^{\frac{\chi_0}{D}H(n) - \frac{\chi_0}{D}c} \right) \right), \end{aligned}$$

because (2.8) implies

$$\frac{\chi_0}{D}H(u) = \log u - \log \left(q(u)/q(1) \right).$$

Our aim is now to use a semi-implicit scheme to solve the time-space discrete version of (2.11) on a square regular grid. For convenience we only present the method in dimension $d = 1$. We first solve the Poisson equation for the chemical potential implicitly: $n(t) \rightarrow c(t + dt)$. Then we discretize (2.11),

$$n_i(t + dt) - n_i(t) = dt \left(\frac{\mathcal{F}_{i+\frac{1}{2}} - \mathcal{F}_{i-\frac{1}{2}}}{dx} \right),$$

where the discrete flux $\mathcal{F}_{i\pm\frac{1}{2}}$ is defined by

$$\begin{aligned} \mathcal{F}_{i+\frac{1}{2}} &= \frac{1}{dx} D \left[q(n)^2(t) \right]_{i+\frac{1}{2}} \exp \left(\frac{\chi_0}{D} \frac{c_{i+1} + c_i}{2} \right) \times \left(\frac{n_{i+1}(t + dt)}{q(n_{i+1}(t))} e^{-\frac{\chi_0}{D}c_{i+1}} \right. \\ &\quad \left. - \frac{n_i(t + dt)}{q(n_i(t))} e^{-\frac{\chi_0}{D}c_i} \right). \end{aligned}$$

For the explicit nonlinear contribution, we choose the geometric mean

$$\left[q(n)^2 \right]_{i+\frac{1}{2}} = q(n_{i+1})q(n_i).$$

In figure 1, we have plotted long time evolution corresponding to $q(u) = 1/(1 + u^\gamma)$ and $q(u) = e^{-\beta u}$. The chemotaxis principle is also valid in the nonlinear case: depending on the parameters (among which high amount of cells and high chemosensitivity favour structure emergence), we observe either cellular aggregation or spread.

Stationary states

Asymptotic behaviours of the linear or non-linear PKS systems (2.1) and (2.5) have been thoroughly analysed by Keller & Segel (1970), Nanjundiah (1973), Childress and Percus (1981) and Schaaf (1985) (see [34]). From these authors' viewpoint, the aggregation principle is related to the instability of the homogeneous steady-state (emergence of spatial structure). More recently, the volume-filling model with the particular saturating function $q(u) = (1 - u/u_{max})_+$ has been studied in dimension one and others [32]. This saturating function corresponds to an infinite valued pressure for large u and can therefore be viewed as a caricatural variant of a more general equation as (2.5). In this case, the formation of plateaus occurs in a fast time scale, then these plateaus merge on a slow time scale [21]. It is proved in [64] that the aggregation principle also holds in this situation: the uniform steady state becomes unstable under some condition similar to $\mu\chi M/D > 8\pi$.

3. Baló's concentric sclerosis: a modeling challenge

The white matter contains the axons of neurons connecting together the cortex, the basal ganglia, the brain stem and the spinal chord. Multiple sclerosis is a chronic demyelinating disease that affects the brain's white matter, and more precisely myelin. Myelin is a fatty substance that surrounds the axons and is necessary for a proper nervous signal transmission. In the central nervous system, myelin is produced by specialized cells, the oligodendrocytes. Several interdependent cellular and molecular processes are involved in demyelination and oligodendrocyte destruction. The neuropathological lesions of MS are plaques (in 2D sections) of demyelinated areas, generally centered on a blood vessel [43].

Baló's concentric sclerosis is a rare and aggressive variant of MS where demyelination regions consists of concentric bands centered by a blood vessel. The process that leads to the formation of such patterns is extremely robust (see figure 2).

The study of BCS may shed some light on the pathogeny of the usual forms of MS. In fact, recent neuropathological studies have pointed out that concentric patterning may occur during the very early stages of most MS cases [5]. Furthermore, epidemiology of Baló's concentric sclerosis shows a clear predominance of this disease in South-East Asia, indicating that concentric demyelination may be caused by some specific genetic predisposition [17]. BCS may thus be an extreme form of MS sharing some common underlying mechanisms with the more usual types of demyelination. In the last section of this paper, we underline the fact that there may exist some positive correlation

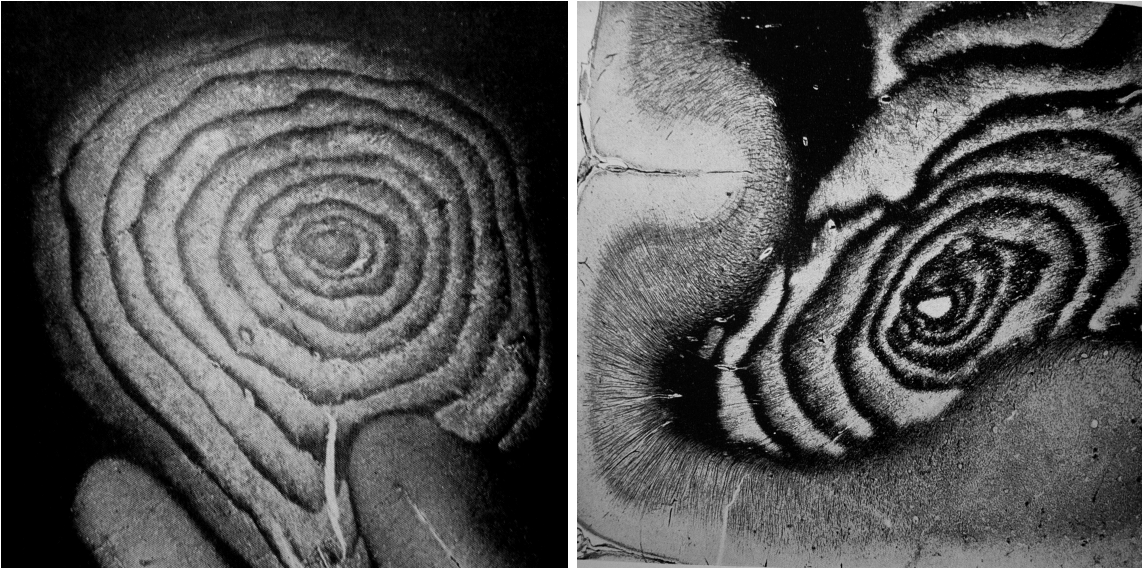


Figure 2. Neuropathology of Baló’s concentric sclerosis from (*left*) Baló 1928 [4] and (*right*) Hallervorden et al. 1933 [29]. The lesional process is remarkably robust, even in constrained areas (*right*). The analysis of these pictures provides morphometric data on the lesions and helps to establish space laws for the pattern.

between cellular aggressivity and spatial organization (as a consequence of the aggregation principle described in section 2). In this context, Baló’s sclerosis may be a subtype of multiple sclerosis in which the cellular aggressivity of demyelinating effectors is unusually increased.

We are convinced that a simple mathematical principle underlies such a robust process. In the next sections, we analyse several models sharing a set of common fundamental hypotheses. One hypothesis is the presence of a propagating front of activation in the brain. The origins of this *leading reaction front* are unknown and its shape varies from one model to another. The link between BCS and LR is based on the presence of this front. In fact, this interesting analogy was suggested and thoroughly studied early in the literature, first by Hallervorden et al. [29]. We reconsider these analogies in the light of the recent discoveries on LR and use this fruitful comparison for the construction of our model.

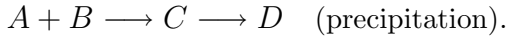
4. Direct concentric patterning

In this section, we present direct pattern processes that do not involve secondary rearrangement scenarios but immediate pattern emergence as the leading reaction front interacts with the medium. The cases in which the pattern is the result of secondary non-linear rearrangements at the back of the propagating front will be studied in the next section.

4.1. Liesegang rings and Ostwald's supersaturation scenario

Liesegang rings, first described by Liesegang in 1896 [44], occur both in chemical processes [30] and in geology [41]. Precipitate rings are the result of chemical interactions between a propagating front and a motionless species. The fact that rings commonly appear in gels, where the viscosity is high, accounts for the necessary reduced mobility of one of the species.

Several scenarios have been proposed to explain periodic precipitation. One of the earliest theories, the so-called *supersaturation* scenario, was formulated by Ostwald in 1897 [51]. Ostwald's supersaturation (OS) involves a single precipitation reaction with an intermediate compound $C = AB$,



The reaction kinetics are based on the existence of two different precipitation thresholds.

Initially, B is uniformly distributed in the gel and A propagates in the domain. Precipitation occurs whenever the concentration of the compound $C = AB$ exceeds the supersaturation threshold q^* and takes place as long as $[AB] > q$ (q being the saturation threshold, with $q < q^*$). Each precipitated band of D depletes the surrounding gel from B by acting as a sink. The presence of two distinct thresholds in the kinetic term ensures that the reaction goes on even when the concentration $[AB]$ is locally below q^* .

Since the early 80's, a lot of works have been dedicated to OS. One of the most intuitive models is probably the one proposed by Keller & Rubinow [38],

$$\begin{cases} \partial_t a &= D_1 a - kab, \\ \partial_t b &= D_2 b - kab, \\ \partial_t c &= D_3 c + kab - P, \\ \partial_t d &= P, \end{cases} \quad (4.1)$$

where the precipitation rate is given by

$$\begin{cases} P = (c - q)_+ & \text{if } d > 0 \text{ or } c \geq q^*, \\ P = 0 & \text{otherwise.} \end{cases}$$

Recently, Hilhorst et al. [31] have derived a simplification of system (4.1) for large reaction rate $k \rightarrow \infty$. In addition they have equivalently reformulated the precipitation rate P as follows,

$$P = (c - q)_+ H \left(\int_0^t (c(s, x) - q^*)_+ ds \right), \quad (4.2)$$

where H denotes the Heaviside function. In other words, as soon as the concentration c is over q^* for some time t_0 , it goes on for $t \geq t_0$ (because $\int_0^t (c(s, x) - q^*)_+ ds > 0$) unless c becomes less than q .

Model 1 (Ostwald’s supersaturation scenario). *In the limit of a fast precipitation reaction between the two species A and B, the concentration compound C satisfies a singular equation,*

$$\frac{\partial c}{\partial t} = \Delta c + \delta(x = \beta t) - P, \quad (4.3)$$

where the precipitation rate P is given by (4.2). The adimensionalized parameters are the speed of the front β and the supersaturation threshold q^* .

We should mention that numerical simulations of equations (4.1) and (4.3) turn out to be difficult (see also [62]). In fact this model belongs to the class of free boundary problems (as the Stefan problem). Recurrent precipitation can be exhibited, however the wavelength of the pattern strongly depends on the space step.

Prenucleation

The Ostwald’s supersaturation scenario is a limiting case of the so-called prenucleation theory where precipitate particles grow in size after their formation (by ‘ripening’), independently from each other [62]. Accordingly, the precipitation rate writes

$$P = \frac{\partial d}{\partial t}, \quad \text{with } d \propto \int_0^t J(s)r(t', t; x)dt', \quad (4.4)$$

the nucleation rate J being function of the supersaturation $s(t, x) = c(t, x)/c_0$. Numerical evidence that such a mechanism eventually leads to recurrent precipitation is given by [20] and [41,42] for example.

Remark 7. *Liesegang rings verify several experimental quantitative space and time laws. The time law states that the position of the n th band x_n is proportional to $\sqrt{t_n}$, where t_n is the time elapsed before the precipitation starts. The spacing law indicates that the ratio between the position of two successive bands converges towards a finite value $1+p$, where $p > 0$. However, these laws are not biologically relevant in the study of BCS [39]. In the following models, the quantitative space and time laws will always depend on the nature of the propagating front.*

4.2. The preconditioning model

The preconditioning hypothesis has been first proposed by Stadelmann et al. [58]. Preconditioning is a theory formulated by biologists interested in ischemia. Cells that find themselves in an ischaemic environment are supposed to produce *preconditioning molecules* (for example heat shock proteins) that protect their neighbouring cells from the deleterious effects of oxygen deficiency. In the scenario of Stadelman et al., a propagating front of oligodendrocyte apoptosis triggers the production and diffusion of molecular signals that protect surrounding oligodendrocytes at the edge of front (see figure 3). The following three-species continuous model is inspired by the qualitative description of [58]. A leading front of a molecular signal $u(t, x)$ activates the microglia and induces the apoptosis of the oligodendrocytes. The density of the damaged cells is $d(t, x)$, whereas the total cell density is a constant denoted by \bar{d} . Attacked cells produce a preconditioning potential $\phi(t, x)$, which diffuses rapidly and protects the cells that have not be damaged yet. The preconditioning potential is active over a range of action compatible with the free diffusion ability of molecules in the brain.

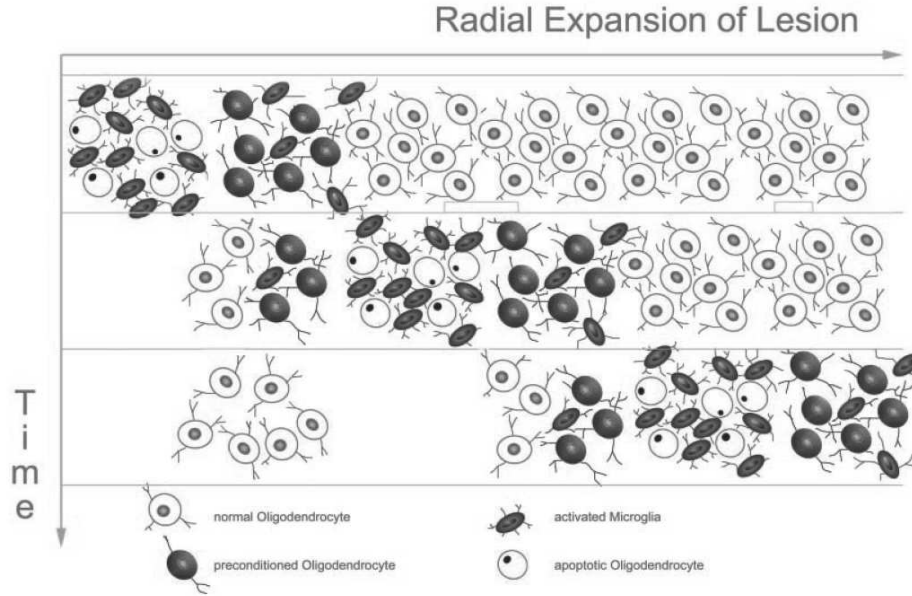


Figure 3. Qualitative description of the preconditioning scenario. The preconditioned oligodendrocytes are not destroyed by the activated microglia (from Stadelmann et al. 2005 [58]).

Model 2 (Preconditioning model). *Let u denote the leading reaction front, d the density of destroyed oligodendrocytes and ϕ the protection potential.*

$$\begin{aligned} \frac{\partial d}{\partial t} &= A(u)P(\phi) (\bar{d} - d), \\ -\varepsilon\Delta\phi + \alpha\phi &= \mu d. \end{aligned} \tag{4.5}$$

The evolution of the outer variable u is not specified (it is a basic traveling front in figure 4).

The protection is expressed by the cut-off function $P(\phi) = (q - \phi)_+$, with a fixed threshold q : if the preconditioning potential is sufficiently high, apoptosis does not occur. The activation term $A(u)$ is typically $H(u - q')$, corresponding to some level set of the leading reaction front. Neither regeneration of oligodendrocytes nor remyelination are taken into account, therefore d can only increase. The potential equation (linear production, natural decay and linear fast diffusion) is chosen to be consistent with our other models. It is still unclear whether preconditioning with this choice for ϕ can lead to the emergence of concentric rings. As a matter of fact, we have numerical evidence that it does not in 1D and in 2D, but this point still requires investigation.

Within system (4.5), an equilibrium is reached at the tip of the moving front (see also [62]). Concentric bands only appear for some formulations of the potential ϕ (see figure 4) which have no biological meaning.

It is worth mentioning that the width of the bands is entirely determined by the range of action of the potential ϕ . However, the wavelength of the BCS patterns (figure 2) is

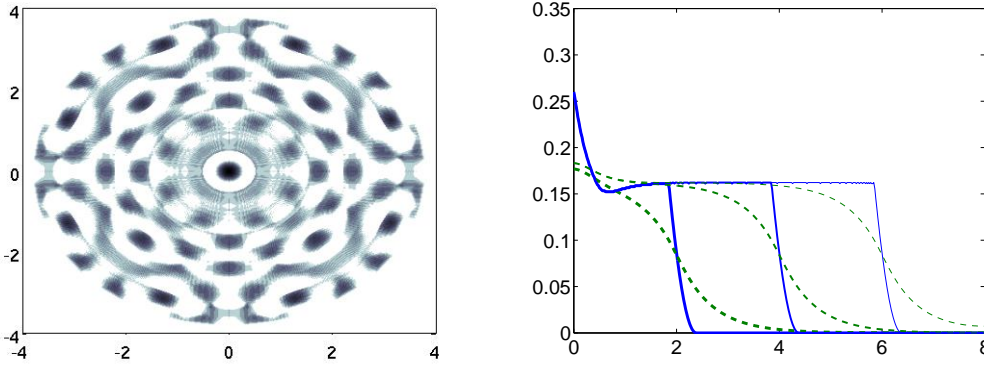


Figure 4. Pattern formation in the preconditioning model 2. (*left*) We replace the potential production in (4.5) by $\phi = K * d$, the kernel K being a stiff Hill function with a range of action equal to $\sqrt{\varepsilon}$: $K(z) = \mathbf{1}_{|z| \leq \sqrt{\varepsilon}}$. Interestingly, the radial symmetry is not preserved. In addition, the pattern wavelength is close to the range $\sqrt{\varepsilon}$. The front speed is $v = 0.1$ and other parameters are $\varepsilon = 0.4$, $q = 0.1$. Very strong preconditioning with $\phi(x) = \max_{|z| \leq \sqrt{\varepsilon}} d(x + z)$ leads to recurrent ring formation where symmetry is conserved. However, the wavelength of such a pattern is not compatible with the biological data. (*right*) In the one-dimensional case, an equilibrium is reached at the front tip. The potential production is driven by $-\varepsilon \Delta \phi + \phi = d$, and parameters are the same as above.

considerably larger than any molecular signal diffusion range known in the brain (see [39] for discussion). It seems thus unlikely that the preconditioning potential could be, as stated by Stadelman et al. [58], the simple resultant of the diffusion of a protective molecule produced by the attacked oligodendrocytes.

The precipitation term in preconditioning is very different from the one used in OS. Indeed, in system (4.1), this rate is notably discontinuous between $d > 0$ and $d = 0$ (this discontinuity is due to the presence of two distinct thresholds, q and q^*). Moreover, in preconditioning, concentric patterns may arise from a temporal discontinuity in the progression of the front: the front may progress, stop, allow the protection to be effective and then start progressing again. The clinical evolution of MS is characterized by the occurrence of attacks, corresponding to demyelination episodes, which could correspond to such temporal discontinuities. However, several MS attacks occurring successively in a few hours period would be necessary to induce concentric demyelination in accordance with pathology's time scales. Such an evolution has never been clinically described.

A concept derived from the prenucleation model (4.4) for LR may help to improve the preconditioning model. By introducing a "maturation in death" effect, damaged oligodendrocytes would die progressively and induce a differential secretion of the signal ϕ . Nevertheless, this new model will not solve the molecular range of action paradox.

5. Secondary rearrangement at the back of the front

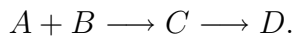
The two models described in this section share the common characteristic of producing patterns behind the leading reaction front. The first one, the competitive coarsening model was first formulated to improve the theoretical description of LR by using a degenerated bistability process. We have already described the second model based on self-attraction of immune cells in our earlier study of BCS [39].

5.1. Postnucleation – The theory of competitive coarsening

Pre- and postnucleation scenarios are extensions of OS based on physical arguments. They both assume that the particles produced by the precipitation reaction have the ability to modify their size at the back of the front. These two theories differ by the supposed nature of the particles (*resp.* solid precipitate and colloid) and the competition mechanism that occurs between growing particles. Postnucleation states that ring formation may be the result of an instability mechanism at the macroscopic level [25]. A more recent model, which will be described below, initially proposed by Feinn et al. [24], involves a two-species instability, namely the growing potential and the local mean radius of particles.

One of the main objections to the direct application of OS to LR formation or concentric demyelination is that in both cases, an area of homogeneous turpitude appears before periodic patterning. In the postnucleation theory, this area corresponds to a non periodic field of colloidal particles and in BCS, to a diffusion anomaly observed with MRI in the white matter before concentric demyelination [63].

The chemical basis of the postnucleation theory is the same as in OS (section 4.1), namely



In addition however, the reaction front induces the formation of colloidal particles (intermediate state between a molecule and a precipitate) by aggregation of the compound $C = AB$ [24]. A colloid is in fact a compound made out of a small number of aggregated molecules, where the surface tension plays a non-negligible role. Spatial structure emerges because large colloids grow faster at the expense of small ones. It is worth noticing that self-organization is driven by the constrain of mass conservation.

The model combines a reaction-diffusion equation for the growing potential with an ODE for the size of the particles. The time and space laws are not taken into account, as mentioned before (remark 7). Accordingly, we build an abstract propagating front with unspecified shape and speed. The concentration of the hypothetical propagating species U is denoted by $u = [U]$. The front forms colloidal particles which are described by a growing potential σ , also called *supersaturation*. The mean colloidal particle size ψ evolves according to a two-sided relaxation towards bistable equilibria (figure 5),

$$\sigma^* = g(\psi) = \frac{2\psi^3}{2\psi^3 + \psi_c^3}.$$

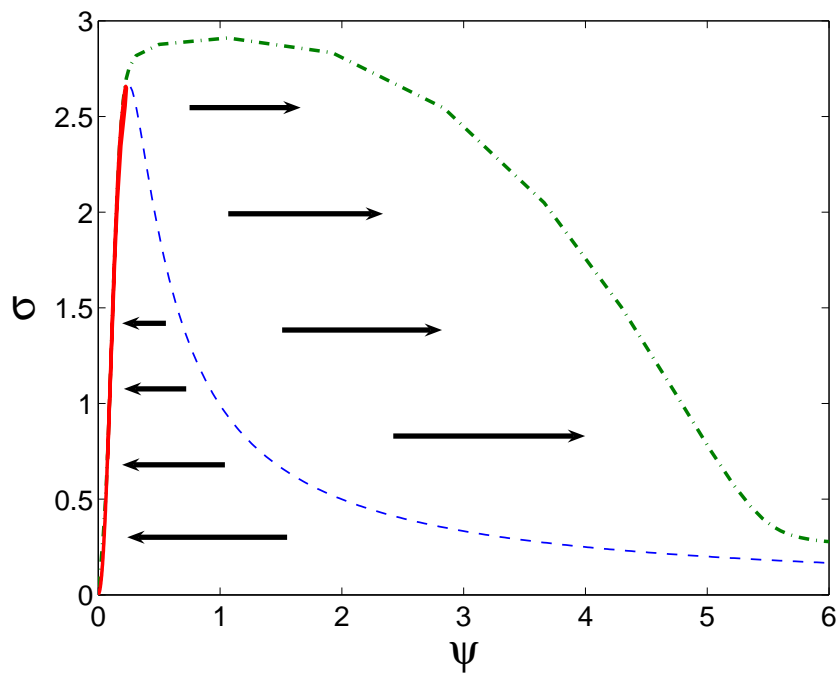


Figure 5. Post-nucleation instability mechanism: the *relaxation* function $g(\psi)$ is plotted in dashed line. In addition, two trajectories in the phase diagram (ψ, σ) are represented in full and dot-dashed lines, corresponding respectively to the black and white arrows in figure 6.

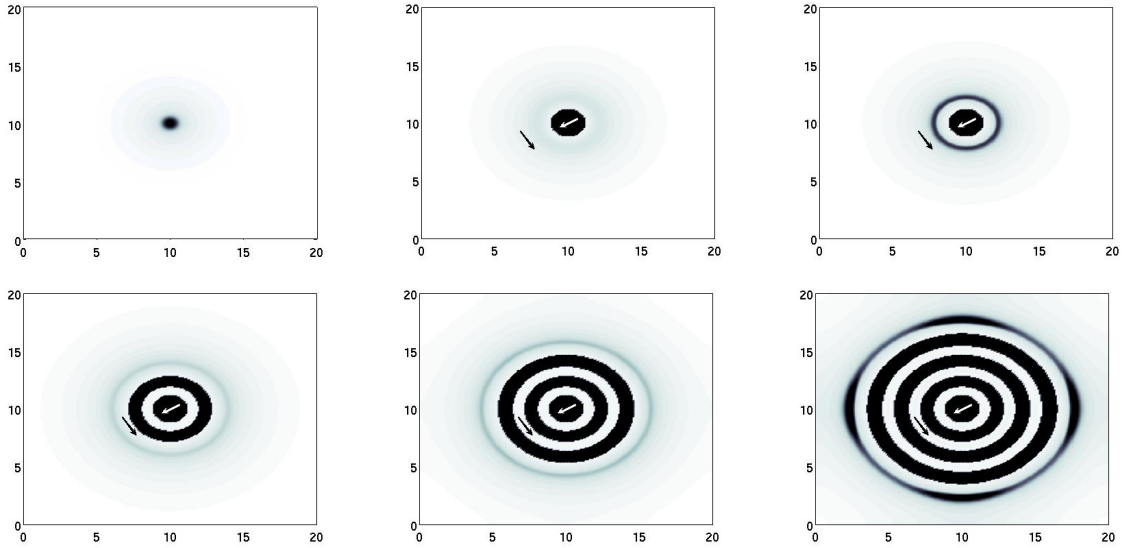


Figure 6. Postnucleation model on a square regular grid: the mean colloidal particle size ψ is successively represented for $t = 22, 30, 32, 42, 53, 64$. The front is Fisher-type, with speed 0.2 and amplitude $A = 10$. Other parameters are $\beta = 0.1$ and $\psi_c = 0.25$ (from Krug et al. [41]). For the black and white arrows, see figure 5.

Model 3 (Post-nucleation). *Let u denote the leading reaction front. The post-nucleation instability writes*

$$\begin{aligned}
 \frac{\partial u}{\partial t} &= \beta \Delta u + Gu(A - u), \\
 \frac{1}{\beta} \frac{\partial \sigma}{\partial t} &= \Delta \sigma - \psi^2 [\sigma - g(\psi)] + u, \\
 \frac{\partial \psi}{\partial t} &= \sigma - g(\psi).
 \end{aligned} \tag{5.1}$$

where ψ denotes the mean particle radius at position x and time t , and σ is the growing potential.

For the sake of coherence with the other models 2 and 4, we have opted for a Fisher reaction-diffusion equation driving the outer activation variable u . We are interested in its amplitude A and its speed $2\sqrt{\beta GA}$. Figure 6 illustrates the evolution of the mean particle size ψ . Note that the rings appear far from the leading front, as a result of the bistable mechanism described in figure 5.

The secondary rearrangement of growing colloids at the back of the front inspired our model for BCS. In this case however, the instability mechanism is driven by chemotaxis.

5.2. Chemotaxis hypothesis for Baló's concentric sclerosis

The mathematical models for morphogenesis were originally based on chemical reactions involving only hypothetical morphogens [60,28]. Such reaction-diffusion mech-

anisms could occur in BCS but we focus our study on self-organization processes due to chemotaxis. The main idea of our model is that organization arises from chemotactic movements in a population of macrophages. The chemical signals attracting the macrophages – supposedly pro-inflammatory molecules – are produced by damaged oligodendrocytes. By recruiting the surrounding macrophages, these oligodendrocytes indirectly protect neighbouring zones.

Model 4 (Local recruitment of macrophages [39]). *Let m be the density of activated macrophages, c the concentration of the attractive signal and d the density of the destroyed oligodendrocytes. The system writes*

$$\frac{\partial m}{\partial t} = D\Delta m + \lambda m(\bar{m} - m) - \nabla \cdot (\chi m(\bar{m} - m)\nabla c) \quad (5.2)$$

$$\frac{\partial d}{\partial t} = F(m)m(\bar{d} - d) \quad (5.3)$$

$$-\varepsilon\Delta c + \alpha c = \mu d, \quad (5.4)$$

where \bar{m} , \bar{d} are characteristic macrophage and oligodendrocyte densities. The damaging function F can be chosen almost arbitrarily as long as it is both positive and increasing. We set $F(m) = \kappa m/(\bar{m} + m)$.

The system reads as follows: macrophages are activated through a Fisher equation and organize chemotactically (5.2), oligodendrocytes are destroyed by activated macrophages (5.3) and produce a chemoattracting signal (5.4). This mechanism leads to concentric band formation at the back of a turpitude area for a wide range of parameters (figure 7). In fact, this model only produces two patterns : concentric bands, as in BCS, and homogeneous plaques of destroyed oligodendrocytes, as in MS (figure 9).

We have opted for a Fisher-type front in (5.2), but the final pattern is independent of this particular choice. Instead we could have used the heat equation accounting for the diffusion of a molecule, or a traveling pulse corresponding to the transduction of some molecular signal (typically cAMP in the modeling of *Dictyostelium*'s aggregation phase [33]). Nevertheless there are quantitative differences between these alternatives (numerical results are shown in figure 8). Furthermore, the analysis of those quantitative differences can provide a suitable test for the selection of the true underlying mechanism which drives macrophages activation (reaction-diffusion, pure diffusion or transduction). The activation front hypothesis raises a controversial point. In fact, one of the main arguments we produced against the preconditioning theory was that the hypothesis of a protective molecule diffusing on centimetric distances was not biologically realistic. In our model the activation front also involves molecular movements on long distances. Nevertheless, no hypothesis is necessary on the nature of this molecule, or on its interactions with the cerebral tissue. There is no particular reason to believe that the propagation of the activation front should be driven by pure diffusion alone. On the other hand, preconditioning involves well characterized molecules which are not known to be involved in specific interactions that would help them to travel through the white matter by any other way than diffusion.

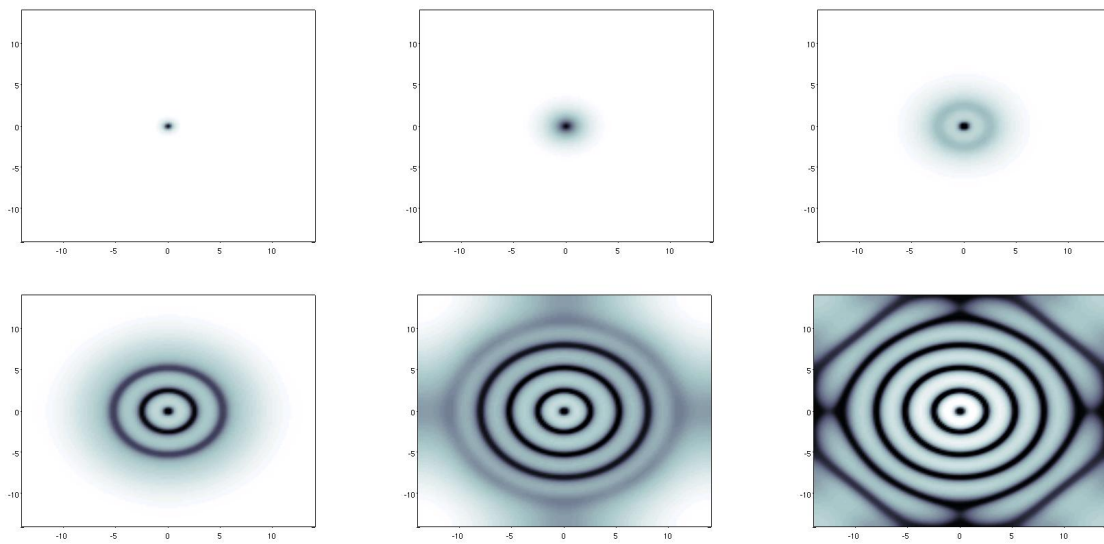


Figure 7. Local recruitment of macrophages: evolution of d (damaged oligodendrocytes) for $t = 1h, 4h, 7h, 10h, 13h, 16h$, from numerical simulations of model 4. Parameters are $r = 2$, $\varepsilon = 0.2$ and $\chi = 30$. The unit length is $L = 1mm$, and the domain width is thus approximately $3cm$. Numerical values for simulations were extracted from [49] and [45]. Destroyed oligodendrocytes are figured in black. Interestingly, successive bands appear behind the edge of the front.

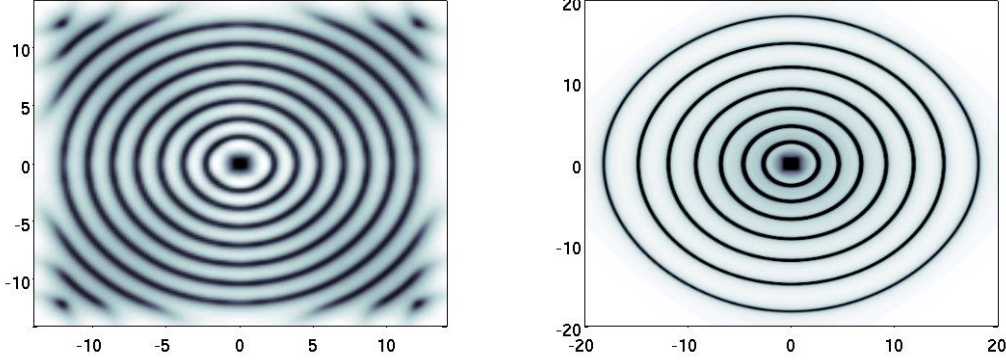


Figure 8. Pattern formation with two different front propagation types: (*left*) the front is a traveling pulse with constant speed, and (*right*) a diffusing molecule activates the macrophages. Note that space and time laws depends on the specific nature of this leading front.

Adimensionalized equations.

We set the reduced variables and parameters as follows,

$$\tilde{m} = \frac{m}{\bar{m}}, \quad \tilde{d} = \frac{d}{\bar{d}}, \quad \tilde{c} = \frac{\alpha}{\mu\bar{d}}, \quad \tau = \lambda\bar{m}t, \quad y = \sqrt{\frac{\lambda\bar{m}}{D}}x, \\ \tilde{\chi} = \frac{\chi\bar{m}\mu\bar{d}}{D\alpha}, \quad \tilde{F}(\tilde{m}) = \frac{\kappa}{\lambda} \frac{\tilde{m}}{1 + \tilde{m}}, \quad \tilde{\varepsilon} = \frac{\varepsilon\lambda\bar{m}}{D\alpha}. \quad (5.5)$$

In particular, the speed of the front and the destructive strenght of the macrophages are balanced by the ratio $r = \kappa/\lambda$. We obtain the following adimensionalized system,

$$\begin{cases} \frac{\partial \tilde{m}}{\partial \tau} = \Delta \tilde{m} + \tilde{m}(1 - \tilde{m}) - \nabla \cdot (\tilde{\chi} \tilde{m}(1 - \tilde{m}) \nabla \tilde{c}), \\ \frac{\partial \tilde{d}}{\partial \tau} = \tilde{F}(\tilde{m}) \tilde{m}(1 - \tilde{d}), \\ -\tilde{\varepsilon} \Delta \tilde{c} + \tilde{c} = \tilde{d}. \end{cases} \quad (5.6)$$

Only three parameters remain, namely the reduced chemosensitivity $\tilde{\chi}$, the reduced chemical diffusivity $\tilde{\varepsilon}$ and the damaging ratio $r = \kappa/\lambda$.

Some qualitative properties of the local macrophages recruitment model

Several qualitative properties are *a posteriori* confirmations of the validity of our model. Local macrophages recruitment model creates concentric patterning, is very robust and allows to draw links between BCS and MS.

The first interesting point is that here, the wavelength of the pattern is not directly related to the range of action of the chemical potential c , as opposed to the preconditioning model 2 (see [39]).

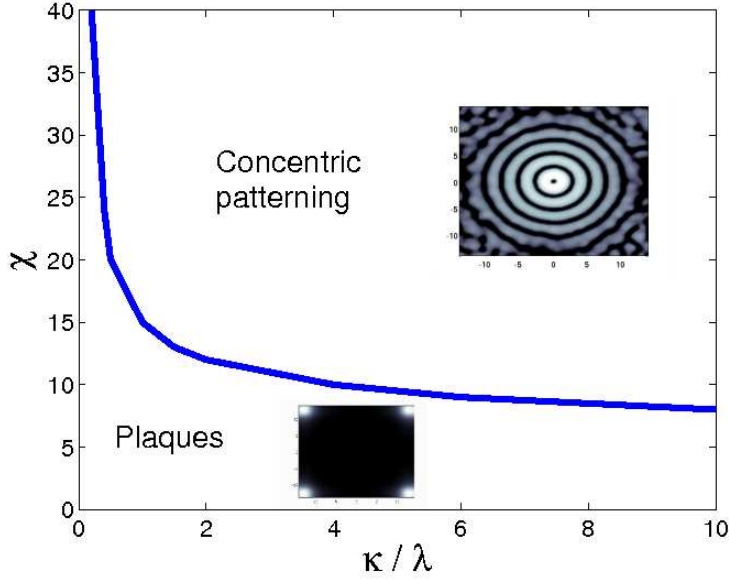


Figure 9. Bifurcation diagram for model 4, with a fixed reduced parameter $\tilde{\varepsilon} = 0.1$. Two situations appear: concentric patterning (structure) or plaques (no structure). Transition between these two states is driven by the structural parameters $\tilde{\chi}$ and r for fixed $\tilde{\varepsilon}$. Concentric patterning is favoured for increasing parameter values: aggressivity is thus positively correlated to spatial structure. The figure in top-right is performed under random perturbation of the chemical diffusivity, showing robustness of the model.

Spatial structuration as a result of aggressivity.

The reduced parameter $\tilde{\chi}$ defined in (2.3) drives the spatial organization of cells in the basic PKS model (2.1), and is also a major parameter in model 4. Consequently, according to the chemotaxis principle (section 2), we expect qualitatively the corresponding $\tilde{\chi}$ in (5.5) to play a similar role. As a matter of fact, by increasing $\tilde{\chi}$, we induce a transition between homogeneous density of damaged oligodendrocytes and concentric patterns (figure 9).

Furthermore, there exists a positive correlation between the aggressivity of the disease and the emergence of structure. The underlying reduced parameter $\tilde{\chi} = \chi \bar{m} \mu \bar{d} / D \alpha$ increases with the aggressivity. Indeed, \bar{m} stands for the amount of immune cells and is in the numerator (note that \bar{m} also appears in the reduced parameter $\tilde{\varepsilon}$, but only because of its role in front speed). As $\tilde{\chi}$ drives the bifurcation between plaques (no structure) and concentric bands (structure), this parameter makes the junction between aggressivity and spatial structure. This assertion is also true for the damaging parameter $r = \kappa / \lambda$, which is related to the macrophages ability to destroy the oligodendrocytes (see figure 9).

Model robustness.

The chemotactic scenario for BCS is highly robust. In fact, our model only produces plaques (no structure) or concentric bands (spatial organization). This simple alternative contrasts with the results of other types of pattern formation models. For instance, in Turing systems, many different patterns can emerge, such as spots or labyrinthic patterns [47,28], depending on the parameters. In models of bacterial colony growth, chemotaxis can lead to localized cellular aggregates [8,61]. Furthermore, another argument that accounts for the robustness of our model is that radial symmetry is well-conserved under different perturbations (see [39] and figure 9).

Short-time assumption.

A major hypothesis of model 4 is that the chemoattractant c is produced by the damaged oligodendrocytes d . This is obviously irrelevant for long evolution times, because the damaged oligodendrocytes are digested by the macrophages. However, we suggest that the relaxation time for macrophages before they re-attack the preserved area is longer than the time scale of concentric demyelination (approximately a few days, BCS is typically aggressive). The macrophages need a "digestion time" before being effective again. This assumption may explain why concentric patterns are observed in very early MS cases [5]. The temporal transition from rings to plaques may first be the result of self-organization (local recruitment), followed by the relaxation of macrophages that spread again in the domain and destroy the pattern to form plaques.

6. Conclusion

Liesegang ring formation and Baló's concentric sclerosis both involve the interaction between a propagating front (whose origin is unknown in BCS) and non-moving molecules or cells. The postnucleation instability in Liesegang rings led us to propose chemotaxis as a self-organization mechanism. The model we built, namely the local macrophages recruitment model, is very robust and closely fits biological data. Three characteristics of our model need further investigations. First, the space and time laws of the pathological process highly depends on the nature of the underlying front. The study of this dependance may help to understand the mechanism of propagation. Secondly, the wavelength of the pattern decreases when the density of macrophages increases. This intuitive statement, based on a refined analysis of chemotaxis-based models, has been numerically verified but still needs theoretical confirmation. Finally, the aggressivity of the disease may account for its structuring ability. BCS may then be a variant of MS where the same general pathogenic mechanisms occur with particular intensity.

The authors address warm thanks to Benoît Perthame for his fruitful help during this work.

REFERENCES

1. W. Alt, Biased random walk models for chemotaxis and related diffusion approximations, *J. Math. Biol.* **9**, 147–177 (1980).

2. A.R.A. Anderson and M.A.J. Chaplain, Continuous and discrete mathematical models of tumor-induced angiogenesis, *Bull. Math. Biol.* **60**, 857–900 (1998).
3. J. Baló, Leucoencephalitis periaxialis concentrica, *Magy Orvosi Arch.* **28**, 108–124 (1927).
4. J. Baló, Encephalitis periaxialis concentrica, *Arch. Neurol. Psychiatr.* **19**, 242–264 (1928).
5. M.H. Barnett and J.W. Prineas, Relapsing and remitting multiple sclerosis: pathology of the newly forming lesion, *Ann. Neurol.* **55**, 458–468 (2004).
6. E. Ben-Jacob, I. Cohen, O. Shochet, A. Tenenbaum, A. Czirók and T. Vicsek, Cooperative Formation of Chiral Patterns during Growth of Bacterial Colonies, *Phys. Rev. Lett.* **75**, 2899–2902 (1995).
7. P. Biler and T. Nadzieja, Existence and nonexistence of solutions for a model of gravitational interaction of particles, *Colloq. Math.* **66**, 319–334 (1994).
8. M.P. Brenner, L.S. Levitov and E.O. Budrene, Physical mechanisms for chemotactic pattern formation by bacteria, *Biophys. J.* **74**, 1677–1693 (1998).
9. E.O. Budrene and H.C. Berg, Dynamics of formation of symmetrical patterns by chemotactic bacteria, *Nature* **376**, 49–53 (1995).
10. H.M. Byrne and L. Preziosi, Modeling solid tumour growth using the theory of mixtures, *Math. Med. Biol.* **20**, 341–366 (2004).
11. V. Calvez and J.A. Carrillo, Volume Effects in the Keller-Segel model: energy estimates preventing blow-up, *J. Math. Pures Appl.* **86**, 155–175 (2006).
12. V. Calvez and Y. Dolak–Struss, Asymptotic Behavior of a two-dimensional Keller-Segel model with and without density control, to appear in *the Proceedings of the sixth ECMTB*, Dresden (2005).
13. V. Calvez and B. Perthame, A Lyapunov function for a two-chemical version of the chemotaxis model, *BIT Num. Math.* **46**(5), 85–97 (2006).
14. V. Calvez, B. Perthame and M. Sharifi tabar, Modified Keller-Segel system and critical mass for the log interaction kernel, to appear in *Contemp. Math.* (2007).
15. E. Carlen and M. Loss, Competing symmetries, the logarithmic HLS inequality and Onofri’s inequality on S^n , *Geom. Funct. Anal.* **2**, 90–104 (1992).
16. F.A.C.C. Chalub, Y. Dolak-Struss, P.A. Markowich, D. Ölz, C. Schmeiser and A. Soreff, Model hierarchies for cell aggregation by chemotaxis, *Math. Mod. Meth. Appl. Sci.* **16**, 1173–1197 (2006).
17. C.J. Chen, N.S. Chu, C.S. Lu and C.Y. Sung, Serial magnetic resonance imaging in patients with Baló’s concentric sclerosis: natural history of lesion development, *Ann. Neurol.* **46**, 651–656 (1999).
18. L. Corrias, B. Perthame and H. Zaag, Global solutions of some chemotaxis and angiogenesis systems in high space dimensions, *Milan J. Math.* **72**, 1–28 (2004).
19. P.D. Dale, P.K. Maini and J.A. Sherratt, Mathematical modelling of corneal epithelium wound healing, *Math. Biosciences* **124**, 127–147 (1994).
20. G.T. Dee, Patterns produced by precipitation at a moving reaction front, *Phys. Rev. Lett.* **57**, 275–278 (1986).
21. Y. Dolak and C. Schmeiser, The Keller-Segel model with logistic sensitivity function and small diffusivity, *SIAM J. Appl. Math.* **66**, 595–615 (2005).
22. J. Dolbeault and B. Perthame, Optimal critical mass in the two dimensional Keller-

- Segel model in \mathbb{R}^2 , *C. R. Math. Acad. Sci. Paris* **339**, 611–616 (2004).
23. F. Filbet, A finite volume scheme for the Patlak-Keller-Segel chemotaxis model, *Numerische Math.* **104**, 457–488 (2006).
 24. D. Feinn, P. Ortoleva, W. Scalf, S. Schmidt and M. Wolff, Spontaneous pattern formation in precipitating systems, *J. Chem. Phys.* **69**, 27–39 (1978).
 25. M. Flicker and J. Ross, Mechanism of chemical instability for periodic precipitation phenomena, *J. Chem. Phys.* **60**, 3458–3465 (1974).
 26. H. Gajewski and K. Zacharias, Global behavior of a reaction-diffusion system modelling chemotaxis, *Math. Nachr.* **195**, 77–114 (1998).
 27. A. Gamba, D. Ambrosi, A. Coniglio, A. de Candia, S. Di Talia, E. Giraud, G. Serini, L. Preziosi, and F. Bussolino, Percolation, morphogenesis, and Burgers dynamics in blood vessels formation, *Phys. Rev. Lett.* **90**, 118101/1–4 (2003).
 28. A. Garfinkel, Y. Tintut, D. Petrasek, K. Boström and L.L. Demer, Pattern formation by vascular mesenchymal cells, *PNAS* **101**, 9247–9250 (2004).
 29. J. Hallervorden and H. Spatz, Über die konzentrische Sklerose und die physikalisch-chemischen Faktoren bei der Ausbreitung von Entmarkungsprozessen, *Arch. Psychiat. Nervenkr.* **98**, 641–701 (1933).
 30. H.K. Henisch, *Crystals in gels and Liesegang rings*, Cambridge University Press, Cambridge, pp. 137–152 (1986).
 31. D. Hilhorst, R. Van der Hout, M. Mimura and I. Ohnishi, personal communication.
 32. T. Hillen and K.J. Painter, Global existence for a parabolic chemotaxis model with prevention of overcrowding, *Adv. Appl. Math.* **26**, 280–301 (2001).
 33. T. Höfer, J.A. Sherratt and P.K. Maini, *Dictyostelium discoideum*: Cellular self-organisation in an excitable medium, *Proc. Roy. Soc. Lond. B* **259**, 249–257 (1995).
 34. D. Horstmann, From 1970 until present: The Keller-Segel model in chemotaxis and its consequences. Part I, *Jahresbericht der DMV* **105**, 103–165 (2003).
 35. W. Jäger and S. Luckhaus, On explosions of solutions to a system of partial differential equations modelling chemotaxis, *Trans. Amer. Math. Soc.* **329**, 819–824 (1992).
 36. D. Julkowska, M. Obuchowski, I.B. Holland and S.J. S  ror, Comparative analysis of the development of swarming communities of *Bacillus subtilis* 168 and a natural wild type: critical effects of surfactin and the composition of the medium, *J. Bacteriol.* **187**, 65–76 (2005).
 37. E.F. Keller and L.A. Segel, Initiation of slime mold aggregation viewed as an instability, *J. Theor. Biol.* **26**, 399–415 (1970).
 38. J.B. Keller and S.I. Rubinow, Recurrent precipitation and Liesegang rings, *J. Chem. Phys.* **74**, 5000–5007 (1981).
 39. H. Khonsari and V. Calvez, The origins of concentric demyelination: self-organization in the human brain, *Plos ONE*, doi:10.1371/journal.pone.0000150 (2007).
 40. R. Kowalczyk, Preventing blow-up in a chemotaxis model, *J. Math. Anal. Appl.* **305**, 566–588 (2005).
 41. H.J. Krug, H. Brandst  dter and K.H. Jacob, Morphological instabilities in pattern formation by precipitation and crystallization processes, *Geol. Rundsch.* **85**, 19–28 (1996).

42. H.J. Krug and H. Brandstädter, Morphological characteristics of Liesegang rings and their simulations, *J. Phys. Chem. A* **103**, 7811–7820 (1999).
43. H. Lassmann, Multiple sclerosis pathology: evolution of pathogenic concepts, *Brain Pathol.* **15**, 217–222 (2005).
44. R.E. Liesegang, Nucleation and colloidal growth in concentration gradients (Liesegang rings), *Photogr. Archiv.* **21**, 221– (1986).
45. C. Lucchinetti, W. Brück, J. Parisi, B. Scheithauer, M. Rodriguez and H. Lassmann, A quantitative analysis of oligodendrocytes in multiple sclerosis lesions – a study of 113 cases, *Brain* **122**, 2279–2295 (1999).
46. N.V. Mantzaris, S. Webb and H.G. Othmer, Mathematical modeling of tumor-induced angiogenesis, *J. Math. Biol.* **49**, 111–187 (2004).
47. J.D. Murray, *Mathematical biology II. Spatial models and biomedical applications*, 3rd edition, Springer-Verlag, New York (2003).
48. T. Nagai, Blow-up of radially symmetric solutions to a chemotaxis system, *Adv. Math. Sci. Appl.* **5**, 581–601 (1995).
49. A. Nimmerjahn, F. Kirchhoff and F. Helmchen, Resting microglial cells are highly dynamic surveillants of brain parenchyma in vivo, *Science* **308**, 1314–1318 (2005).
50. Oberwolfach Report **24**, *Mathematical Biology*, Mathematisches Forschungsinstitut Oberwolfach (2006).
51. W. Ostwald, *Lehrbuch der allgemeinen Chemie*, Engelmann, Leipzig (1897).
52. K.J. Painter, P.K. Maini and H.G. Othmer, Stripe formation in juvenile *Pomacanthus* explained by a generalised Turing mechanism with chemotaxis, *PNAS* **96**, 5549–5554 (1999).
53. K.J. Painter and T. Hillen, Volume-filling and quorum-sensing in models for chemosensitive movement, *Can. Appl. Math. Q.* **10**, 501–543 (2002).
54. C.S. Patlak, Random walk with persistence and external bias, *Bull. Math. Biophys.* **15**, 311–338 (1953).
55. B. Perthame, PDE models for chemotactic movements: parabolic, hyperbolic and kinetic, *Appl. Math.* **49**, 539–564 (2004).
56. L. Preziosi (Ed.), *Cancer Modelling and Simulation*, Chapman Hall/CRC Press (2003).
57. D. Scharfetter and H. Gummel, Large signal analysis of a Silicon Read diode oscillator, *IEEE Trans. Electron Devices* **16**, 64–77 (1969).
58. C. Stadelmann, S. Ludwin, T. Tabira, A. Guseo, C.F. Lucchinetti, L. Leel-Ossy, A.T. Ordinario, W. Brück and H. Lassmann, Tissue preconditioning may explain concentric lesions in Baló’s type of multiple sclerosis, *Brain* **128**, 979–987 (2005).
59. M. Tessier-Lavigne and C.S. Goodman, The molecular biology of axon guidance, *Science* **274**, 1123–1133 (1996).
60. A.M. Turing, The chemical basis of morphogenesis, *Phil. Trans. R. Soc. London B* **237**, 37–72 (1952).
61. R. Tyson, S.R. Lubkin and J.D. Murray, Model and analysis of chemotactic bacterial patterns in a liquid medium, *J. Math. Biol.* **38**, 359–375 (1999).
62. G. Venzl and J. Ross, Nucleation and colloidal growth in concentration gradients (Liesegang rings), *J. Chem. Phys.* **77**, 1302–1307 (1982).
63. H. Wiendl, R. Weissert, U. Herrlinger, H. Krapf and W. Kuker, Diffusion abnor-

- mality in Baló's concentric sclerosis: clues for the pathogenesis, *Eur. Neurol.* **53**, 42–44 (2005).
64. D. Wrzosek, Long-time behaviour of solutions to a chemotaxis model with volume-filling effect, *Proc. Roy. Soc. Edinburgh A* **136**, 431–444 (2006).
 65. X. Yang, D. Dormann, A.E. Munsterberg and C.J. Weijer, Cell movement patterns during gastrulation in the chick are controlled by positive and negative chemotaxis mediated by FGF4 and FGF8, *Dev. Cell* **3**, 425–437 (2002).